Prediction of wire-EDM Process Parameters for Surface Roughness using Artificial Neural Network and Response Surface Methodology

Machaieie, Ana Tiago[1], Byiringiro, Jean Bosco[2] and Njiri, Jackson Githu[3]

***Abstract*— The prediction of machining process capabilities is important in process parameter optimization and improvement of machining performance characteristics. This paper, presents the prediction of Wire-EDM input parameters for surface roughness using Artificial Neural Network and Response Surface Methodology. Ti-6Al-4V is an alpha-beta alloy widely applied in industry due of its excellent combination of mechanical properties. However, this alloy is found to be difficult to machine by means of conventional machining processes because of its high melting temperature, high chemical reactivity, and low thermal conductivity. Nevertheless, non-conventional machining processes such Wire-EDM are able to overcome the challenge in machining Ti-6Al-4V. Response Surface Methodology (RSM) based on Central Composite design is used to evaluate and optimize the effect of pulse on time (*Ton*), discharge current (*I*) and open circuit voltage (*UHP*) on surface roughness (*SR*). Analysis of Variance revealed that open-circuit voltage is the most significant parameter affecting the obtained surface roughness followed by the discharge current. Parametric variation shows that lower surface roughness can be obtained at lower levels of *UHP and I*. The main contribution of this paper is the prediction of wire-EDM machining process parameters for a given surface roughness using Artificial Neural Network (ANN). The developed ANN model revealed to be 97.155% accurate with an average prediction error of 2.845%. The predictive capability of the developed ANN model is found to be satisfactory and the model can be successfully used for predicting machining process parameters for desired surface roughness in wire electrical discharge machining process.**

***Index Term*— Artificial Neural Network, Response Surface Methodology, Scan Electron Microscopy, Ti-6Al-4V, WEDM**

I. INTRODUCTION

WIRE Electrical Discharge Machining is a thermo-electrical machining process consisting of a continuous traveling vertical-wire electrode, in which the material removal is due to spark erosion between the workpiece and the wire immersed in an electrically non-conductive dielectric fluid [1]–[6].

This work was financially supported by Pan African University, Institute for basic Sciences, Technology and Innovation, Nairobi – Kenya. The experiments were conducted in Stellenbosch University - Stellenbosch Technology Centre, South Africa.

Machaieie, A.T. is with the Mechanical and Mechatronics Engineering Department, Pan African University, Institute for basic Sciences, Technology and Innovation, Nairobi – Kenya. (phone: 254716870069, e-mail: anathiagomachaieie@gmail.com).

Byiringiro J.B. is with the Mechatronics Engineering Department, Dedan Kimathi University of Technology, Nyeri – Kenya. (e-mail: jean.bosco@dkut.ac.ke).

Njiri, J. G. is with the Mechatronics Engineering Department, Jomo Kenyatta University of Agriculture and Technology, Nairobi – Kenya. (e-mail: jackgithu@eng.jkuat.ac.ke).

Wire electrical discharge machining has the ability to machine precise, complex and irregular shapes of difficult to machine electrically conductive components. With this process, titanium alloy, alloy steel, conductive ceramics and aerospace materials can be machined irrespective of their hardness and toughness [3], [4], [6]–[8].

The Wire-EDM spark erosion process is due to the increase of voltage between the workpiece and wire electrode, causing the intensity of the electric field in the gap to be greater than the strength of the dielectric, resulting in electrical breakdown. The electrical breakdown allows the current to flow between the two electrodes, forming a plasma channel and spark discharges and therefore removing material from the workpiece. During pulse off-time, new dielectric fluid is flushed into the machining gap, serving as a coolant, enabling the debris to be carried away and restoring the insulating properties of the dielectric [1], [2], [4], [7].

The performance of WEDM is mainly evaluated in terms of material removal rate, surface finish, and sparking gap. Surface finish plays a very critical role in manufacturing engineering for determining the quality of engineering components, which can have an influence in their performance and in production costs. Various failures of components, sometimes catastrophic, leading to high costs, have been attributed to the poor surface finish of the components in question. A high surface quality improves the fatigue strength, corrosion and wear resistance of the component [1], [8]–[12].

Wire electrical discharge machining provides an effective solution for machining hard materials with intricate shapes. However, the selection of optimum parameters for the machining process is still a challenge. This is because wire-cutting parameters for obtaining higher cutting accuracy and improved surface finish in WEDM is still not fully solved [1], [2], [4].

Titanium alloys are regarded as important engineering materials for industrial applications due to their outstanding combination of properties such as high strength-to-weight ratio, low density, high elastic stiffness, good fracture toughness, excellent resistance to corrosion, good fatigue resistance and biocompatibility [1], [10], [13]. They are widely used in various fields such as aerospace, military, marine, biomedical, chemical, power generation, sporting goods, automobile, electronic, gas and food industry [10], [11], [14], [15]. Titanium alloy grade 5 (TI-6Al-4V) is an alloy belonging to the group of alpha-beta titanium alloys, considered five times more resistant than steel [1],[14],[11]. TI-6Al-4V is the most popular metal among titanium alloy group because of its wide application in industry, specially marine and aerospace [6], [7]. However, these alloys have relatively high melting temperature, low thermal conductivity and high electrical resistivity compared to other common materials[1], [11], [14], which make their machining difficult [10], [13] costly, and requiring specialized cutting tools [13],[14],[16]. Machining titanium alloys by conventional

machining methods result in rapid tool wear because of their low thermal conductivity and high chemical reactivity which result in high cutting temperature at the cutting zone and strong adhesion between the cutting tools and the material [3], [9], [14]. For these reasons, there have been research developments with the objective of optimizing the cutting conditions of Titanium alloys to obtain an improved machining performance.

S. Ramesh, L. Karunamoorthy, and K. Palanikumar [9] investigated the effect of cutting parameters on the surface roughness in turning process of titanium alloy grade 5 using response surface methodology. The investigated parameters were cutting speed, feed rate, and depth of cut. The results showed that feed rate was the most influential factor affecting the surface roughness. The investigated effect on surface roughness was done during turning process, the effect of the parameters on surface roughness during Wire-EDM was not part of the scope, therefore parameters such as pulse on time, discharge current and open circuit voltage were not investigated.

S. Ramesh, L. Karunamoorthy, and K. Palanikumar [10] developed a surface roughness model of WEDM process of Titanium alloy in terms of cutting parameters such as cutting speed, feed, and depth of cut using response surface methodology and ANOVA. The results indicated that the feed rate is the main influencing factor on surface roughness, where it increased with the increase of feed rate, but decreased with the increase of cutting speed and depth of cut. However, in this study was not considered the influence of parameters such as pulse on time, discharge current and open circuit voltage on surface roughness. The scope of this study also did not include the prediction of machining processes.

D. Ghodsiyeh, A. Davoudinejad, M. Hashemzadeh, N. Hosseininezhad, and A. Golshan [1] investigated the influence of peak current, pulse on-time and pulse off-time on Surface Roughness (SR), Material Removal Rate (MRR) and Sparking Gap (SG) in WEDM of Ti-6Al-4V using response surface methodology. Peak current was found to be the most important factor for surface roughness and material removal rate while Pulse on time was the most significant for sparking gap. In this study was not considered the influence of open circuit voltage on surface roughness and the methodology did not explore the prediction of machining processes.

Nourbakhsh *et al.* [14] investigated the effect of process parameters including pulse width, servo reference voltage, pulse current, and wire tension on process performance parameters such as cutting speed, wire rupture and surface integrity in WEDM of titanium alloy using Taguchi design, ANOVA and Scan electron microscopy. It was found that the cutting speed increases with increase of peak current and pulse interval. Surface roughness increased with increase of pulse width and decreased with increase of pulse interval. This study did not consider the influence of pulse on time on surface roughness, application of response surface methodology and the prediction of machining processes.

Saedon *et al.* [6] studied the influence of peak current (IP), feed rate (FC) and wire tension (WT) to cutting speed and surface roughness of Ti-6Al-4V in WEDM using Response Surface Methodology. The cutting rate obtained ranged between 3.9 mm/min and 9.8 mm/min, where the maximum was obtained when the parameters were set at peak current (12 A), feed rate (12 mm/min) and wire tension (16 N). The surface roughness obtained ranged from 1.667 μm to 3.018 μm, where the minimum was obtained for combination as given by peak current (1.27 A), feed rate (8 mm/min) and wire tension (11 N). In this study was not considered the effect of pulse on time and open circuit voltage on surface roughness, neither the prediction of machining processes.

A. Prasad, K. Ramji, and G. L. Datta [2] investigated the effect of peak current, pulse on-time, pulse off-time and servo reference voltage on material removal rate and surface roughness using Taguchi method and analysis of variance. The most significant parameters for both MRR and SR were found to be peak current and pulse on-time, whereas pulse off-time and servo reference voltage were less effective factors. It was also observed that both MRR and SR increase and decrease simultaneously. The study did not consider response surface methodology and the prediction of machining processes.

Rahman [3] investigated the effect of peak current, servo voltage, pulse on-time and pulse off-time on material removal rate (MRR), tool wear rate (TWR) and surface roughness (SR) in EDM using artificial neural network. It was observed that peak current effectively influences the performance measures. The results indicated that the proposed ANN model can satisfactorily evaluate the MRR, TWR as well as SR in EDM. The proposed model was to predict the machining performance in WEDM while varying the input parameters. It was not considered the prediction of machining process parameters to obtain a given or desired performance.

B. Pradhan and B. Bhattacharyya [17] modeled the micro-electro-discharge machining process of Ti-6Al-4V using response surface methodology and artificial neural network algorithm. The studied parameters are peak current, pulse on-time and dielectric flushing pressure. The optimal combination of process parameters settings obtained are pulse-on-time of 14.2093 ms, peak current of 0.8363 A, and flushing pressure of 0.10 kg/cm2 for achieving the desired Material Removal Rate, Tool Wear Rate, and Overcut. During this study, it was not considered the effect of the parameters on surface roughness. The artificial neural network model developed was for prediction of machining performance using different process parameters, it was not considered the reverse process, where from a known, given or desired machining performance it is predicted the required machining process parameters for the machining process.

The main contribution of this paper is the prediction of wire-EDM machining process parameters to obtain a desired surface roughness using Artificial Neural Network and Response Surface Methodology. This allows one to conduct machining processes and obtain the desired or required performance, leading to better surface quality, reducing product failures; and reducing the machining time, increasing productivity.

II. Response Surface Methodology

Response surface methodology (RSM) is a collection of mathematical and statistical techniques based on the fit of a polynomial equation to the experimental data, which must describe the behavior of a data set with the objective of making statistical previsions. They are useful for the modeling and analysis of problems in which a response of interest is influenced by several variables and the objective is to optimize this response [9], [10], [18], [19].

A. Variables Screening

Many variables may affect the response of a system, however it is necessary to select those variables with major effects for the modeling.

B. Choice of the Experimental Design

Response surface modeling is built on the approximation of the correct performance of a response. The model response is expressed as

$$y = f(\theta_1, \theta_2, \theta_3, \ldots . \theta_k) + \varepsilon \quad (1)$$

where $\theta_1, \theta_2, \theta_3, \theta_k$ represent the variables and ε represent the residual related to the experiments.

The elementary model used in response surface methodology, is a linear function expressed as

$$y_i = \beta_0 + \sum_{i=1}^{k} \beta_i x_i + \varepsilon \quad (2)$$

where k represents the number of variables, β_0 is the average value of y_i, β_i represents the first order coefficients, and x_i constitute the coded factors of the variables.

Therefore, the responses of this model do not present a curvature. To assess curvature, a second-order model describing the interaction between different variables, which is expressed as

$$y_{ij} = \beta_0 + \sum_{i=1}^{k} \beta_i x_i + \sum_{1 \le i \le j}^{k} \beta_{ij} x_i x_j + \varepsilon \quad (3)$$

where β_{ij} constitute the interaction coefficients. The interaction model evaluates the curvature, however to determine a critical point, the polynomial function must contain quadratic terms as

$$y_{ii} = \beta_0 + \sum_{i=1}^{k} \beta_i x_i + \sum_{1 \le i \le j}^{k} \beta_{ij} x_i x_j + \sum_{i=1}^{k} \beta_{ii}^2 x_i + \varepsilon \quad (4)$$

where β_{ii}^2 represents the second-order coefficients. To evaluate the parameters in Eqn. 4, a two-modeling symmetrical response surface design such as the central composite design has to be used to ensure that all studied variables are affected in at least three factor levels.

C. Level of the variables codification

Codification of the variables helps to analyze variables of different magnitude, where the evaluation of the variable of greater magnitude does not influence the evaluation of the variable of lesser magnitude. The coded value is obtained as

$$x_i = \frac{\theta_i - \theta_{min}}{\delta\theta/2} - 1 \quad (5)$$

where, θ_i is the real variable value, x_i is the coded value, θ_{min} is the minimum variable value and $\delta\theta$ is the variable range.

D. Mathematical analysis of the data

In matrix notation, Eqn. 2 - Eqn. 4 is represented as

$$y = Xb + e \quad (6)$$

where y is a nx1 response vector, X is a nxp matrix of the coded values named design matrix, b is a px1 vector of the model coefficients, and e is a nx1 vector of the model residuals. A column of ones is added to the design matrix for the determination of the average value of y.

After the design matrix is built, the model residual is determined using the Method of Least Squares (MLS), which minimizes the error between the observed and predicted values. The model residual is obtained as

$$e = y - \hat{y} \quad (7)$$

where e represents a nx1 vector of the model residuals, y represents a nx1 vector of the observed response values, and $\hat{y}$ represents a nx1 vector of the predicted response. The predicted response is obtained as

$$\hat{y} = Xb \quad (8)$$

After mathematical transformations of Eqn. 8, the sum of squares of the model residuals is minimized according to

$$\frac{\partial e'e}{\partial b}(y - Xb)'(y - Xb) = \cdots = -2X'y + 2X'Xb = 0 \quad (9)$$

where the vector of model coefficients is obtained as

$$b = (X'X)^{-1}X'y \quad (10)$$

Equation 10 is the least square estimate (LSM) of b. Because of the random distribution of the errors, it is necessary to estimate the variance of each component of b by genuine repetitions of the central point as

$$\hat{V}_b = (X'X)^{-1}s^2 \quad (11)$$

Accordingly, the standard errors for the coefficients of b are obtained by the extraction of the square root for each component of $\hat{V}_b$, making possible to assess its significance.

E. Assessment of the fitted model

The assessment of the fitted model is authentically done by the application of analysis of variance (ANOVA) [8], [14], [20]. Analysis of variance compares the variation explained by the model with the variation of model residuals, thus evaluating the significance of the regression model used for predictions in comparison to the real data. The assessment of the data variation is done by studying its dispersion. The evaluation of the square deviation d_i^2 that each observation (y_i) or its replicates (y_{ij}) present in relation to the media ($\bar{y}$) is computed as

$$d_i^2 = (y_{ij} - \bar{y})^2 \quad (12)$$

The total sum of the square (SS_{tot}) is the sum of squares of all observations associated to the media, and is presented as

$$SS_{tot} = \sum_{i=1}^{n}(y_i - \bar{y})^2 = SS_{reg} + SS_{res} \quad (13)$$

where (SS_{reg}) is sum of squares due to regression and (SS_{res}) is sum of squares due to the residuals. The sum of the squares due to residuals can be subdivided into sum of the square due to pure error (SS_{pe}) and sum of the square due the lack of fit (SS_{lof}), and presented as

$$SS_{res} = \sum_{i=1}^{n}(y_i - \hat{y}_i)^2 = SS_{pe} + SS_{lof} \quad (14)$$

The model sum of squares is given by the sum of the square (SS_{tot}) and residuals generated by the model (SS_{res}) as

$$SS_{mod} = SS_{tot} + SS_{res} \quad (15)$$

The pure error is given by

$$SS_{pe} = \sum_{i=1}^{m}\sum_{j=1}^{nr}(y_{ij} - \bar{y}_i)^2 \quad (16)$$

where SS_{pe} is the estimate of a pure error, nr is the number of replicas at a design location and m is the number of design locations where replicas were performed. The sum of the square due the lack of fit (SS_{lof}) can also be obtained from

$$SS_{lof} = SS_{res} - SS_{pe} \quad (17)$$

Fisher's distribution is used to compare the variation of the regression media squares and the variation of the residuals media squares while considering the degrees of freedom (dof) associated to these squares as

$$\frac{MS_{reg}}{MS_{res}} \approx F_{V_{reg},\, V_{res}} \quad (18)$$

where the square media of regression is represented as (MS_{reg}), the squares media of residuals as (MS_{res}), the dof related to the regression as (V_{reg}) and the dof related to

residuals as (V_{res}). If the F_{test} presents a value greater than the tabulated F value means that the experimental data is well explained by the regression model and the model is considered statistically significant. The lack of fit test is also used as an alternative for evaluating the significance of the regression model where it is expected that it becomes insignificant, because it is desirable to fit the data. The lack of fit test is descried as

$$\frac{MS_{lof}}{MS_{pe}} \approx F_{V_{lof,Vpe}} \quad (19)$$

$$R^2 = \frac{SS_{mod}}{SS_{tot}} = 1 - \frac{SS_{res}}{SS_{tot}} \quad (20)$$

where R^2 is the coefficient of determination. Its weakness is that it continues increasing as more terms are added to the model, leading to over-fitting. To solve this problem, it is introduced the adjusted R-squared which takes into account the degrees of freedom in the model, decreasing as the model terms are added if the model fit does not increase and increasing as terms are added if the model fit also increase. The adjusted R-squared is described by

$$R^2_{adj} = 1 - (SS_{res}/(n-p) * (n-1)/SS_{tot}) \quad (21)$$

F. Determination of optimal conditions

The optimal conditions of a linear model are determined by the direction indicated by the generated surfaces. For quadratic models, the optimal conditions are calculated based on the first derivate of the regression equation described as

$$y = b_0 + b_1x_1 + b_2x_2 + b_{12}x_1x_2 + b_{11}x_1^2 + b_{22}x_2^2 \quad (22)$$

To obtain the optimal conditions the quadratic equation has to be differentiated as described by

$$\frac{\partial y}{\partial x_1} = b_1 + 2b_{11}x_1 + b_{12}x_2 = 0 \quad (23)$$

$$\frac{\partial y}{\partial x_2} = b_2 + 2b_{22}x_1 + b_{12}x_1 = 0 \quad (24)$$

Therefore, to determine the optimal points, it is necessary to solve the first grade system formed by Eqn. 23 and Eqn. 24, after finding x_1 and x_2 values, then substitute in Eqn. 22.

III. EXPERIMENTAL PROCEDURES

Experimental design constitute a systematic method concerning the planning of experiments, collection, and analysis of data with near-optimum use of available resources [8], [10]. During this study, experiments were carried out in Stellenbosch University - Stellenbosch Technology Centre, South Africa.

A. Experimental Setup

In this paper, Ti-6Al-4V is used as a workpiece, deionized water as dielectric fluid and a brass wire of 0.25mm as the wire electrode. Table I provides the information of experimental conditions used during the machining process.

TABLE I
Experimental Conditions for the machining process

Condition	Description
Workpiece	10mmx10mmx10mm Ti-6Al-4V
Tool Electrode	Brass wire, 0.25mm
Dielectric	Deionized Water
Polarity	(workpiece "+ve", wire "-ve")
Flushing Pressure (bar)	0.3/8 bar
Pulse frequency	3/50
Constant feed rate (mm/min)	0.01
Advancing Wire (mm/sec)	135
Force Wire (N)	17
Pulse on-time (ms)	15.6-46.8
Discharge current (A)	102-170
Open circuit voltage (V)	108-326

Fig. 1. Wire cut +GF+ Agie Charmilles CA 20

Figure 1 shows the WEDM machine used in this study. A number of experiments were carried out according to the design of experiment (DOE) generated by RSM based on central composite face-centered design to investigate the influence of pulse on-time, discharge current and open-circuit voltage on surface roughness.

B. Work material

Cubes of Ti-6Al-4V alloy are machined by WEDM (wire cut +GF+ Agie Charmilles CA 20). Ti-Al-4V has the following chemical composition, Titanium (Ti= 89.58%), Aluminum (Al= 6%), Vanadium (V= 4%), Carbon (C < 0.10%), Oxygen (O<0.20%), Nitrogen (N< 0.05%), Hydrogen (H < 0.0125%), Iron (Fe < 0.3%) [2], [13], [17], [21].

C. Experimental Design

The Response Surface Methodology based on Central Composite Design was used for the evaluation and optimization the effect of machining process parameters on

surface roughness. The central composite design employed is face-centered, which means that alpha (α) is equal to 1.
Alpha is the distance of each star or axial point from the center. This variety of design requires 3 levels of each factor. Thus, the total number of experimental runs is 20. The three variables controlled in this paper are pulse on-time (Ton), discharge current (I), and open-circuit voltage (UHP), with minimum and maximum values of 15.6 to 46.8 ms, 102 to 170 A, and 108 to 326 V respectively. Table II illustrates the experimental design consisting of 8 factorial design points, 6 center points and 6 axial points. The center points allow the experimenter to obtain an estimate of the experimental error and to obtain a more precise estimate of the effects. The experiment was performed randomly to satisfy analysis of variance requirements for random distribution of errors.

TABLE II
Central Composite Design table - Response Surface Methodology

Run	Ton (ms)	I (A)	UHP (V)	SR
1	31.2	136	217	0.755
2	31.2	136	326	0.78
3	31.2	102	217	0.567
4	46.8	170	326	1.4
5	15.6	170	326	0.94
6	31.2	136	217	0.59
7	31.2	136	217	0.82
8	46.8	102	108	0.355
9	31.2	136	217	0.554
10	46.8	170	108	0.425
11	15.6	136	217	0.678
12	31.2	136	217	0.59
13	15.6	102	326	0.456
14	46.8	102	326	0.8
15	31.2	136	217	0.71
16	31.2	170	217	0.535
17	15.6	170	108	0.759
18	31.2	136	108	0.725
19	46.8	136	217	0.71
20	15.6	102	108	0.63

IV. Results and Discussions

A. Response Surface Model

The developed two-parameter interaction model for the surface roughness for the machining process of Ti-6Al-4V is explained by

$$SR = 0.6903 + 0.0231Ton + 0.1247I + 0.1456UHP + 0.0076TonI + 0.1761TonUHP + 0.1111UHP \quad (25)$$

TABLE III
Model Summary of the fit Statistics

R-squared	0.9541
Adjusted R-squared	0.9296
Predicted R-squared	0.7813
Adequate Precision	11.9212

Table III presents the model summary of the fit statistics. The R-squared of 0.9541 is close to 1, which indicates that the model is effective in explaining the experimental data. The adjusted R-squared reveals that the model fit takes into account the degrees of freedom and is not led by over-fitting of the parameters. The Predicted R-squared of 0.7813 is as close to the Adjusted R-squared of 0.9296 as expected, presenting a difference less than 0.2 [1], [8], [14], consequently they are in reasonable agreement.
Adequate Precision computes the signal to noise ratio, by comparison of the predicted values to the average prediction error. Because it is desirable to obtain a ratio above 4, then the obtained ratio of 11.9212 implies appropriate model discrimination. Figure 2, presents the optimum parameters for surface roughness. The goal set was to minimize the surface roughness while maintaining the variables in the range.

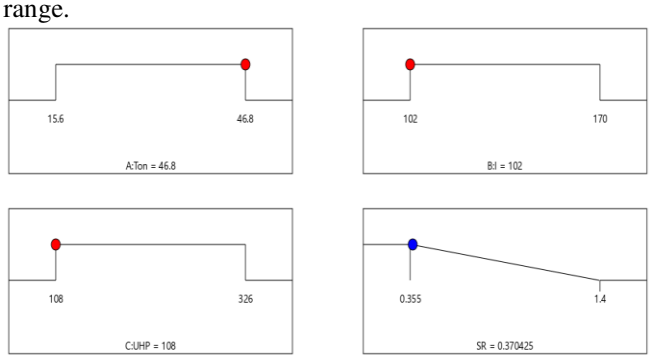

Fig. 2. Surface roughness optimization

The optimization process is according to Eqn. 22 - Eqn. 24 and it helps to identify the combination of Ton, I, and UHP that jointly optimize the surface roughness. The desirability assesses how well the combination of these variables satisfies the goal defined that is to minimize the surface roughness. The desirability ranges from 0 to 1 and an optimal solution is found when it is at his maximum. The minimum surface obtained is 0.3704 μm with the Ton, I and UHP equal to 46.8ms, 102 A, 108 V respectively.

B. Analysis of variance

Analysis of Variance was used to estimate the suitability of the regression model given in Eqn. 25, employing F-test for the determination of the significance of the model considering the variance of all the terms at a suitable level of α. The F-test evaluation is based on the null hypothesis, which states that all coefficients of the regression equation are equal to zero against the possibility that at least one of the regression coefficients is not equal to zero. Analysis of Variance (ANOVA) was used to determine the statistical reliability of the suggested relationship between the parameters pulse on time, discharge current and open circuit voltage and the response, the surface roughness.
Table IV presents the Analysis of Variance results. The quadratic terms were all found to be insignificant, so they were removed and the adopted model is a two-interaction model. Throughout analysis, it was used a confidence level of 95%, which indicate that the significance, α is equal to 0.0500. The significance of the model was verified by the Fishers F-test. The Model F-value of 7.24 indicate that the model is significant and there is only a 0.15% chance that this large F-value could be a result of noise. The P-values less

than the value imply significance of the model terms. In this case I, UHP, TonxUHP, and IxUHP are found to be significant model terms. Contrarily, Ton, TonxI are found to be insignificant because present p-values greater than 0.1000. The effect of open-circuit voltage is the most significant factor associated with surface roughness based on its p-value. The Lack of Fit presents a F-value of 1.71 and a p-value of 0.2865 which indicates that the lack of fit of this model is not significant relative to the pure error, and there is only a 28.65% chance that this large F-value of lack of fit could be a result of noise. A non-significant lack of fit is good because it desirable that the model fits. Therefore, the two-interaction model is found to be well fitted because it reveals to have a significant regression and insignificant lack of fit.

TABLE IV
Analysis of variance

Source	DF	SS	MS	F-Value	p-Value
Model	6	0.7202	0.12	7.24	0.0015
Ton	1	0.0053	0.0053	0.32	0.5802
I	1	0.1555	0.1555	9.38	0.0091
UHP	1	0.212	0.212	12.8	0.0034
TonxI	1	0.0005	0.0005	0.03	0.8696
TonxUHP	1	0.2482	0.2482	15	0.0019
IxUHP	1	0.0988	0.0988	5.96	0.0297
Residual	13	0.2155	0.0166		
Lack-of-Fit	8	0.1579	0.0197	1.71	0.2865
Pure Error	5	0.0576	0.0115		
Total	19	0.9936			

C. Model Diagnostic Checking

Model diagnostic checking is a method used to analyze the model residuals based on certain assumptions in order to confirm the ANOVA results, which avoids to obtain misleading results. One of the diagnostic checking assumptions is done by building a normal probability plot of the residuals, where every residual is plotted versus its expected value under normality. It is expected to obtain a straight-line plot, with emphasized central points than the extremes, indicating that the residual distribution is normal. Another checking is the residual independence assumption done by plotting the residuals according to the order of runs in data collection. This plot should not present obvious patterns. During diagnostic checking it is also checked the assumption of constant variance by plotting the residuals against the predicted values, which is satisfied if the plot is structureless [1], [8], [14]. The model diagnostic checking has been done and the results are presented from Fig. 3 - Fig. 6. The normal probability plot is presented in Fig. 3. The obtained results indicate that the errors are distributed normally because the residuals fall on a straight line.

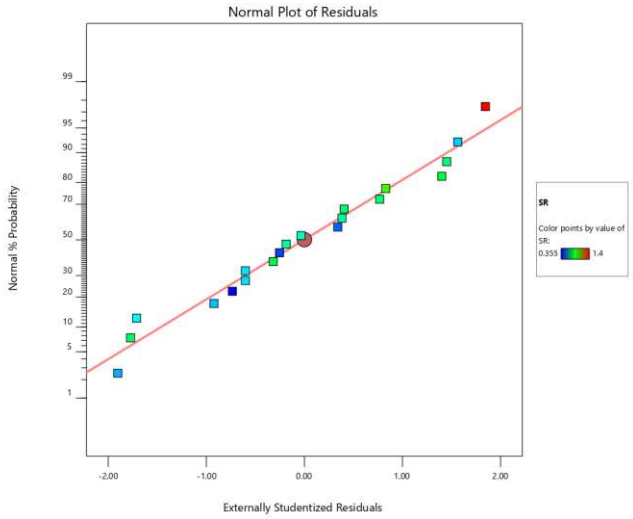

Fig. 3. Normal plot of the RSM model residuals

Figure 4 presents the plot of the standardized residuals against the predicted values. The residuals do not show any obvious pattern and are distributed in both positive and negative directions, which satisfies the assumption of constant variance.

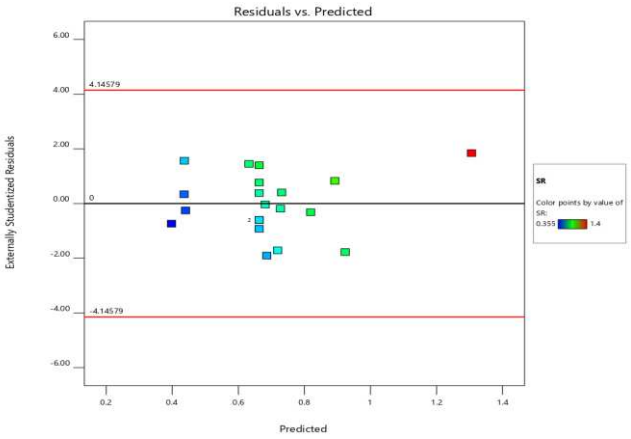

Fig. 4. Relationship between standardized residuals and predicted values in RSM

Figure 5 presents the plot of the residuals against the time order of runs of data collection. The plot does not present obvious pattern, implying that the independence of assumption on the residuals was not violated and the model is adequate.

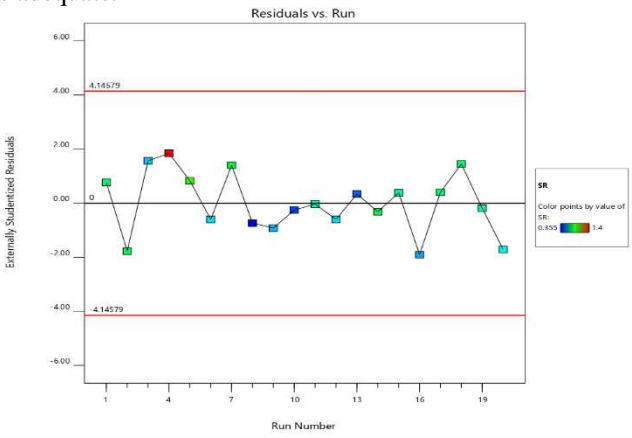

Fig. 5. Plot of the residuals against the time order of runs

Figure 6 presents the plot of the experimental values against the predicted values of surface roughness. Most of the points fall on the straight line and the experimental are very close to predicted values implying that the evaluation and prediction provided by the model is reliable.

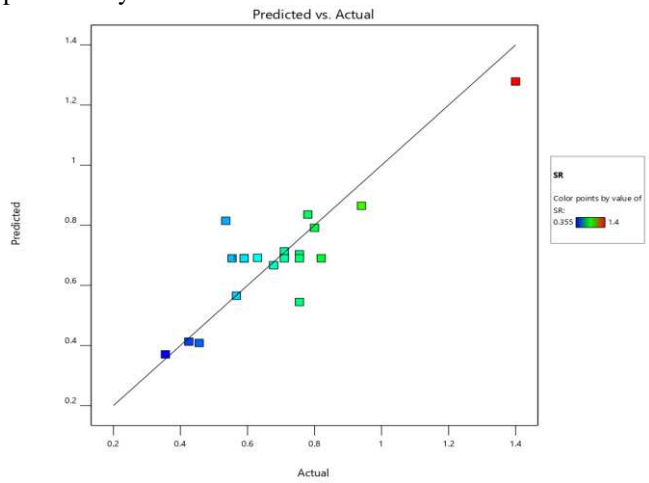

Fig. 6. Relationship between actual and predicted values using RSM

The analysis of surface roughness are explained through 2D contour plots and 3D surface plots. The contour plots show how the values of the surface roughness change as a function of two variables of the process parameters, while the third variable is held constant [10]. All the points with the same surface roughness are joined to build contour lines of constant surface roughness. The surface plot helps to examine the relationship between the surface roughness and two parameters while the third parameters is held constant by viewing a 3D surface of the predicted surface roughness.

It allows to examine the relationship between two parameters jointly and the response and also the relationship between each parameter and the surface roughness. The peaks and valleys represent the combination of two machining process parameters that produce local maximum and local minimum respectively. The contour plots and surface plots for surface roughness regarding the machining process parameters are shown from Fig. 7 - Fig. 12.

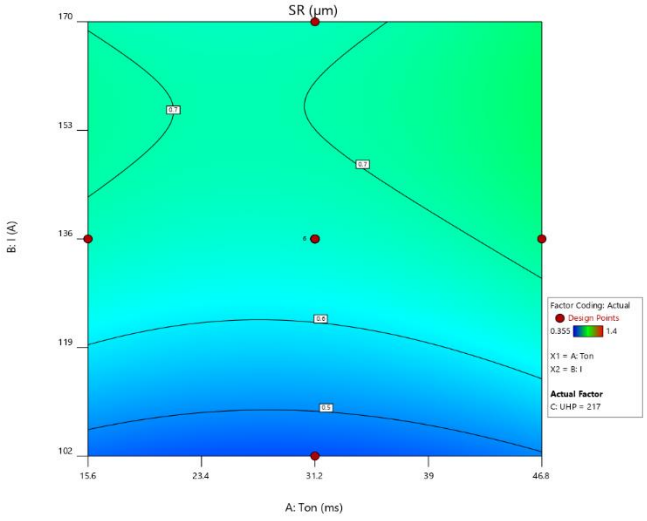

Fig. 7. Contour plot of the relationship between the parameters Ton, I and the Surface Roughness

Figure 7 presents the contour plot of the relationship between parameters Ton and I and Surface Roughness. At low values of I even when the T on is increased to its maximum, the contour obtained is low, of about 0.5 μm. Maintaining the values of T on and increasing the values of I the surface roughness increases to about 0.6 μm. At low values of T on and high values of I the surface roughness increases and a contour of 0.7 μm is obtained. At high values of Ton and high values of I the surface roughness still increases to about 0.7 μm. This means that the effect of T on is not significant to the obtained surface roughness and that in this interaction of Ton and I, the I is the most influential parameter on the surface roughness.

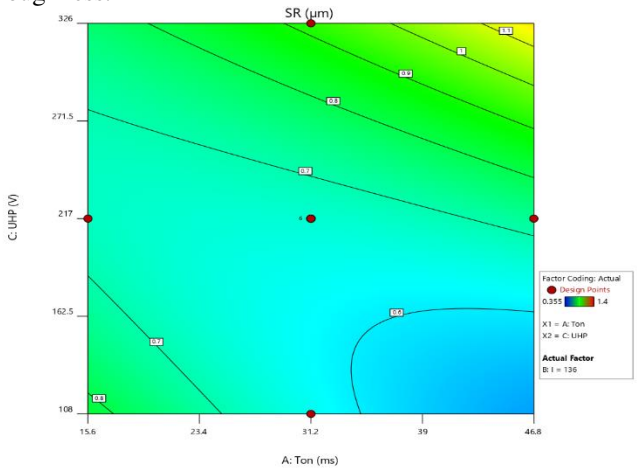

Fig. 8. Contour plot of the relationship between parameters Ton, UHP and the Surface

Figure 8 presents the contour plot of the relationship between the parameters Ton, UHP and the Surface Roughness. At low values of UHP and high values of T on is obtained the minimum surface roughness for this interaction which is about 0.6 μm. At high values of T on and high values of UHP the maximum surface roughness for this interaction is obtained, contour of 1.1 μm. However, the high values of T on still produce a low surface of 0.6 but the low values of UHP produce a surface roughness of 0.8 μm, then the high surface roughness attained at the high values of both parameters is attributed to the UHP not Ton.

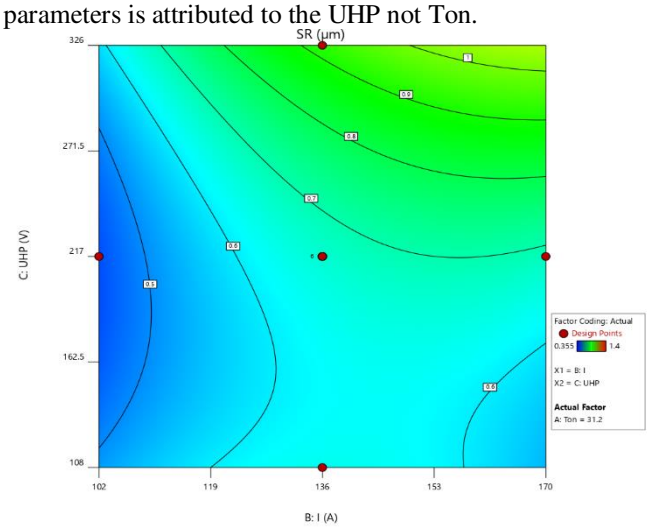

Fig. 9. Contour plot of the relationship between parameters I, UHP and the Surface Roughness

Figure 9 present the contour plot of the relationship between parameters I, UHP and the Surface Roughness. At low values of UHP and high values of I is obtained the minimum surface roughness for this interaction which is about 0.6 μm. At high values of UHP and low values of I is also obtained the minimum surface roughness for this interaction which is about 0.6 μm. At low values of UHP and low values of I is obtained the low surface roughness which is about 0.6 μm.
At high values of I and high values of UHP the maximum surface roughness for this interaction is obtained, which range from 0.7 μm to 1.1 μm. Therefore, it is observed that the parameters UHP and I conflict with each other in a way that in this interaction there is no one parameter that is more influential than the other, but the significance in the entire model is attributed first to the UHP according to the ANOVA and then followed by the I.

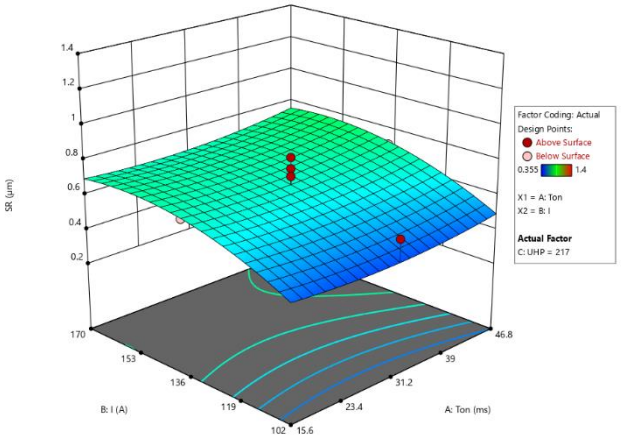

Fig. 10. Surface plot of the relationship between parameters Ton, I and the Surface Roughness

Figure 10 presents the surface plot of the relationship between parameters Ton, I and the Surface Roughness Surface which is an additional analyze to the analysis provided in Fig. 7. Figure 10 shows that when Ton is increased the surface roughness is increased to a range of 0.4 μm - 0.6 μm. When I is increased, the surface roughness is increased to a range of 0.6 μm - 0.6 μm. The increase in the interaction of the two parameters produces a surface roughness in a range of 0.6 μm - 0.8 μm, which means that the affecting parameter here is the I and the interaction of the two parameters is not significant to the model as revealed in the ANOVA results.

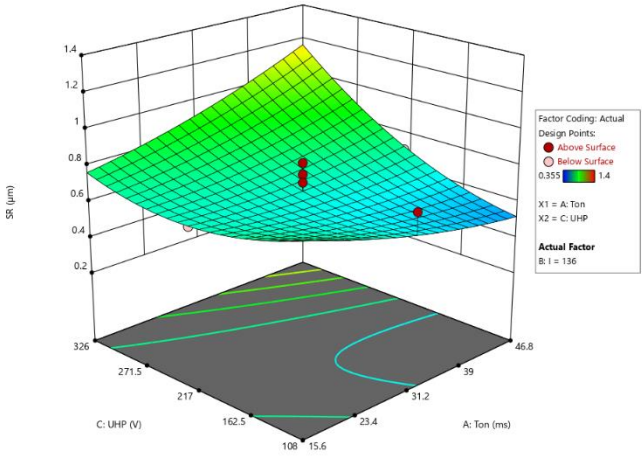

Fig. 11. Surface plot of the relationship between parameters Ton, UHP and the Surface

Figure 11 presents the surface plot of the relationship between parameters Ton, UHP and the Surface Roughness, which is an additional analyze to the analysis provided in Fig. 8. Figure 11 shows that when Ton is increased the surface roughness is increased to a range of 0.4 μm - 0.6 μm. When UHP is increased, the surface roughness is increased to a range of 0.6 μm - 0.8 μm. The increase in the interaction of the two parameters produces peak or local maximum and increases the surface roughness to a range of 1.0 μm - 1.2 μm, which means that the more affecting parameter here is the UHP, however the interaction of the two parameters is significant to the model as revealed in the ANOVA results.

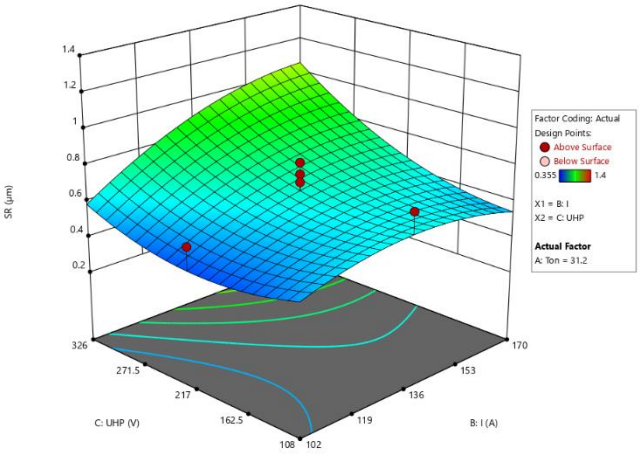

Fig. 12. Surface plot of the relationship between parameters I, UHP and the Surface Roughness

Figure 12 presents the surface plot of the relationship between parameters I, UHP and the Surface Roughness which is an additional analyze to the analysis provided by Fig. 10. Figure 12 shows that when I is increased the surface roughness is increased to a range of 0.4 μm - 0.6 μm. When UHP is increased, the surface roughness is increased to the same range but closer to 0.6 μm. The decrease in the interaction of the two parameters produces valley or local minimum and the increase in the interaction produces peak or local maximum and increases the surface roughness to a range of 1.0 μm - 1.2 μm, which means that the two parameters and their interaction is significant to the model but the UHP is more significant than the I as revealed in the ANOVA results.

The contour plots and the surface plots of the relationship between parameters Ton, I, and UHP and the Surface Roughness reveal that the most significant parameter affecting the surface roughness is UHP followed by I as presented in the ANOVA results. Low values of I and UHP minimize the obtained surface roughness and high values of I and UHP maximize the obtained surface roughness.

D. Scan Electron Microscopy analysis results

Wire-EDM machined samples with different surface roughness from the preliminary experiment and main design of experiment were selected and prepared for Scan Electron Microscopy (SEM) analysis. The objective of this scan was to analyze the morphology, the micro-structure, and composition of the samples of different roughness machined at different machining parameters levels after the machining process. Figure 13 - Fig. 17 describe the sample preparation process. The samples previously machined in WEDM were cut using a sewing machine as in Fig. 13 to allow the analysis of the cross-sectional area.

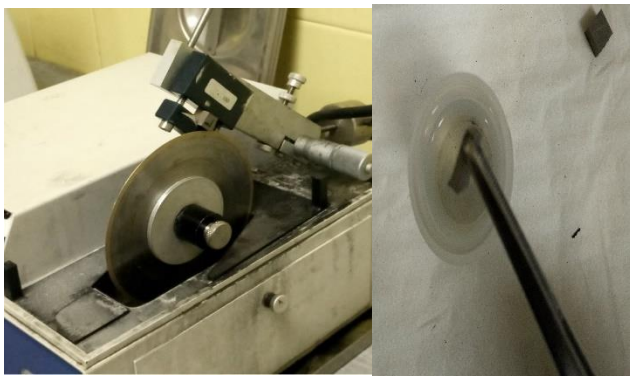

Fig. 13. Sample Preparation: Sawing process

They were mounted in an automatic mounting press using epomet molding compound, at a pressure of 280bar, heat time of 3.50 minutes and cool time of 4.00 minutes as shown in Fig.14.

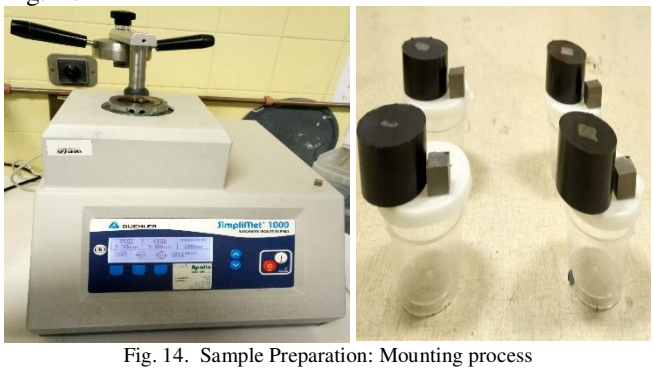

Fig. 14. Sample Preparation: Mounting process

Later on, they were grinded and polished on a 2speed grinder-polisher to remove the peaks and obtain an even surface as shown on Fig. 15.

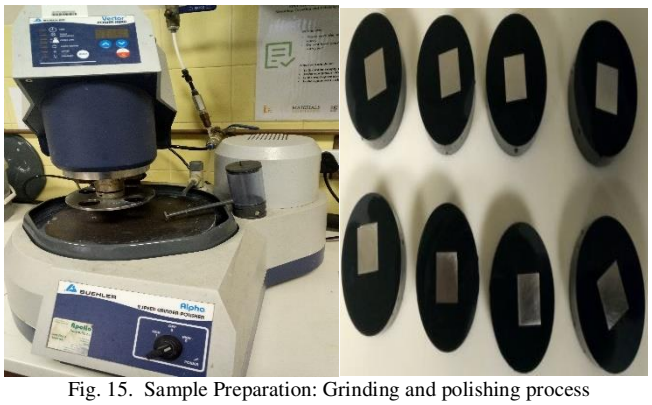

Fig. 15. Sample Preparation: Grinding and polishing process

The non-mounted samples cut on the sewing machine were ultrasonically cleaned as shown on Fig. 16 with acetone and the mounted samples were cleaned with acetone only before the itching process.

Fig. 16. Sample Preparation: Ultrasonic cleaning process

Lastly all the samples were itched with a solution of 2wt% HF / 20wt% HNO3 (based on Kroll's reagent) for about 15 seconds and rinsed in distilled water.

Fig. 17. Sample Preparation: After Itching process

The samples were analyzed using the scan electron microscopy Gemini 2 as presented in Fig. 18.

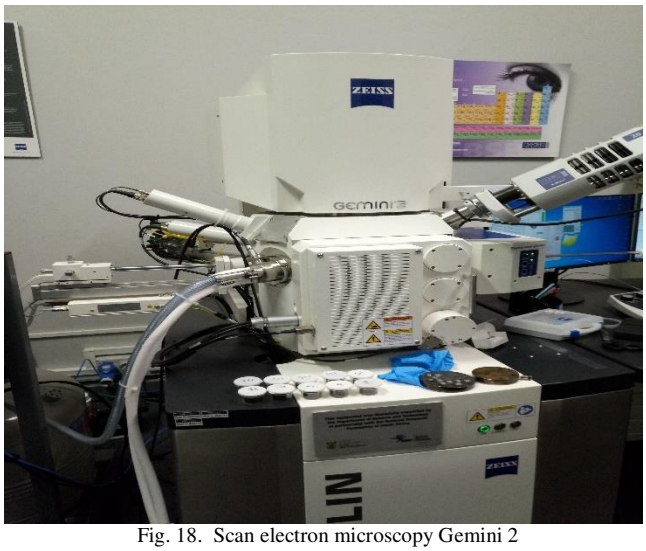

Fig. 18. Scan electron microscopy Gemini 2

After the preliminary evaluation of the scan electron microscopy analysis of the wire-EDM machined samples, it was selected one sample of a lower surface roughness (0.590 μm), one sample of an average surface (1.440 μm) and one sample of a higher surface (3.150 μm- obtained in the preliminary experiment) machined at the different levels of process parameters for deeper analysis of their morphology, micro-structure and composition. The scan electron microscopy analysis of the three samples in terms of morphology, heat affected zone, white layer, and composition is presented below.

i. Analysis of the morphology

Figure 19 - Fig. 21 show the SEM analysis of the morphology of the machined surfaces of Ti6Al-4V done in a working distance (WD) of 9.5mm; magnified 1000 times (Mag=1.00 KX).

Figure 19 presents a sample machined at Ton=31.2 ms, I= 136 A, UHP = 217 V, with a resultant surface roughness of 0.590 μm. The sample presents smaller crater sizes, smaller cracks, smaller melted drops, and a smoother surface that resulted from the average discharge current (level 2), average open-circuit voltage (level 2) and average pulse on-time (level 2).

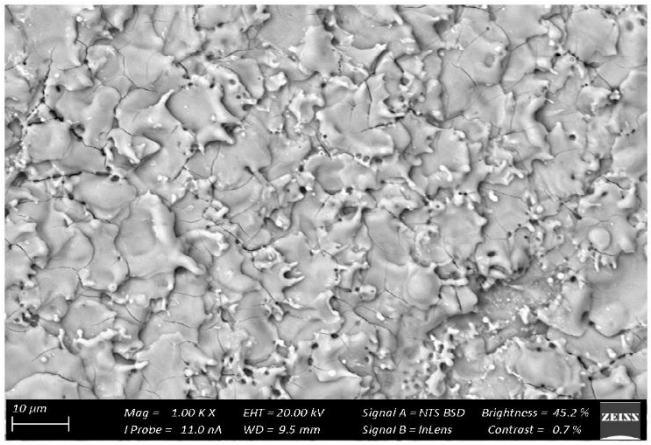

Fig. 19. SEM analysis of the morphology of the machined Ti-6Al-4V with surface roughness of 0.590 μm

Figure 20 presents a sample machined at Ton=15.6 ms, I= 102 A, UHP = 326 V, with a resultant surface roughness of 1.440 μm. As the pulse on time is decreased to level 1, discharge current is decreased to level 1, and the open circuit voltage is increased to level 3. It is observed an increase in the surface roughness, the melted drops become bigger, also the cracks and craters. This agrees with the analysis of variance results obtained from the response surface methodology that the obtained surface is more influenced by the open circuit voltage than the other two parameters.

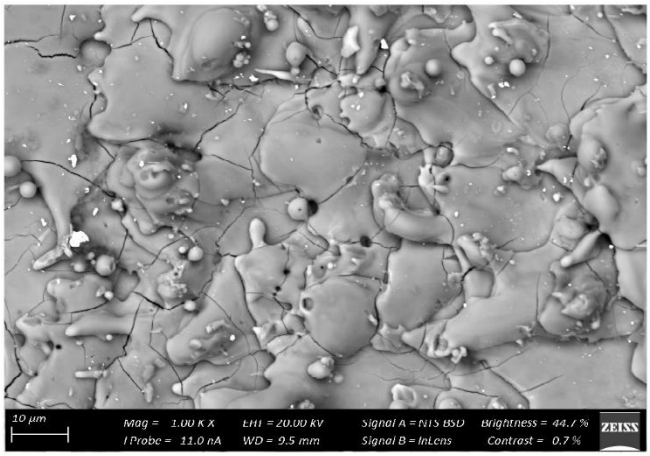

Fig. 20. SEM analysis of the morphology of the machined Ti-6Al-4V with surface roughness of 1.440 µm

Figure 21 presents a sample machined at Ton=500 ms, I= 578 A, UHP = 54 V, with a resultant surface roughness of 3.150 μm. This sample was obtained during the preliminary experiment; therefore, its values are not within the levels defined in the design of experiment. Figure 21 shows bigger crater sizes, bigger cracks and bigger melted drops, consequently a very rough surface. Primarily, the parameter setting was not optimized, and from the result of the previous morphologies in the Fig. 19 and Fig. 20, this proves that the response surface design and its optimization of process parameters improves significantly the obtained surfaces in wire electrical discharge machining process. Secondly, though this experiment presents a huge pulse on time, the morphology cannot be resultant of it because the first two morphologies demonstrated that the pulse on time was not significant, as obtained in the analysis of variance, as it was decreased from Fig. 19 to Fig. 20 but still the cracks, craters and drops kept increasing. The morphology is more attributed to the open circuit voltage as seen in the previous figures and analysis of variance, but as also seen in the interaction of discharge current and open circuit voltage in Fig. 12, these two parameters conflict which eat other. Therefore because of that, the obtained surface can be more attributed to discharge current applied in the machining process, rather than the open circuit voltage.

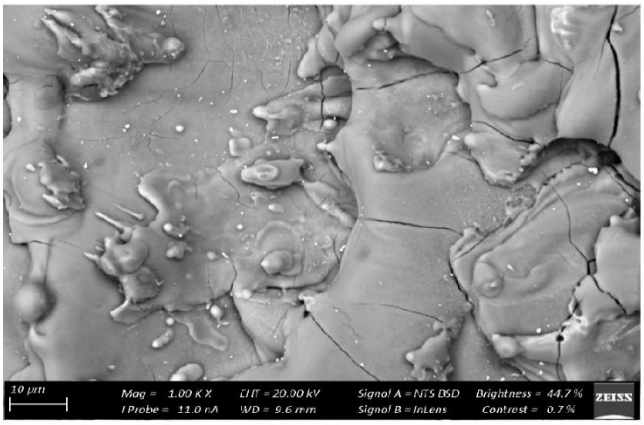

Fig. 21. SEM analysis of the morphology of the machined Ti-6Al-4V with surface roughness of 3.150 µm

In the analysis of the morphology was observed that as the surface roughness increases, the melted drops, the craters and the cracks also increase. The main factor that contributed to the increase of the surface roughness is the open circuit voltage and the discharge current.

ii. Heat Affected Zone and White Layer analysis

The wire electrical discharge machining melts the workpiece material, and part of the melted metal is flushed away during the pulse off-time. However, the left molten material re-solidifies forming a recast layer known as white layer because of its white appearance under the microscope. Below the white layer, it is formed a heat affected zone as a result of the rapid heating and cooling cycles of the wire electrical discharge machining process [5], [16]. The SEM images in Fig. 22, Fig. 23, and Fig. 24 display the heat affected zone and the white layer created during the machining process. The SEM images were analyzed using Fiji Image-J software to measure the thickness of the heat affected zone and the white layer.

Figure 22 presents a sample machined at Ton=31.2ms, I= 136 A, UHP = 217 V, with a resultant surface roughness of 0.590 μm. The white layer thickness obtained in Fig. 22 is 0.013mm and the heat affected zone corresponds to 0.027 mm. Fig. 22 reveals smaller white layer thickness and a lower heat affected zone resulted from the average discharge current, average open-circuit voltage and average pulse on-time applied during the machining process.

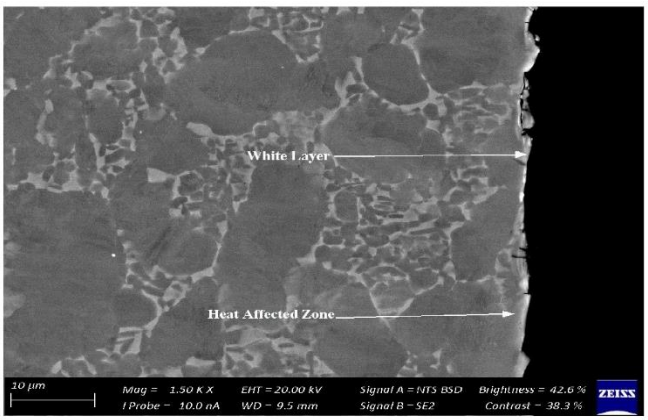

Fig. 22. SEM analysis of the heat affected zone and white layer of the machined Ti-6Al-4V with surface roughness of 0.590 μm

Figure 23 presents a sample machined at Ton=15.6 ms, I= 102 A, UHP = 326 V, with a resultant surface roughness of 1.440 μm. The white layer thickness obtained in Fig. 23 is 0.016 mm and the heat affected zone corresponds to 0.043 mm. By comparing Fig. 22 and Fig. 23 it is observed the major effect of open circuit voltage on the white layer thickness, although the discharge current is influencing significantly the heat affected zone.

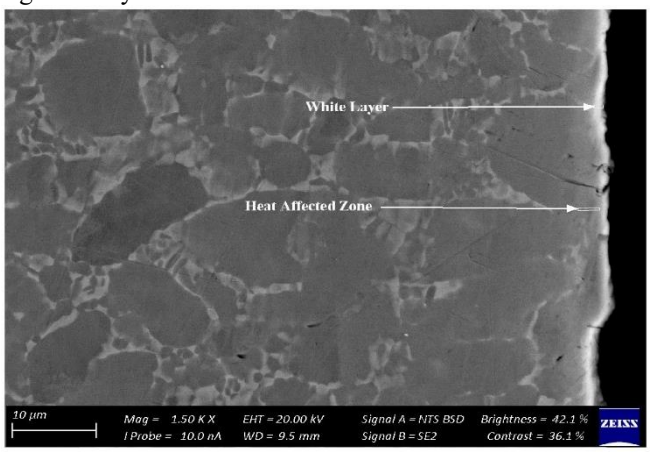

Fig. 23. SEM analysis of the heat affected zone and white layer of the machined Ti-6Al-4V with surface roughness of 1.440 µm

Figure 24 presents a sample machined at Ton=500 ms, I= 578 A, UHP = 54 V, with a resultant surface roughness of 3.150 μm. The white layer thickness obtained in Fig. 24 is 0.021 mm and the heat affected zone corresponds to 0.081 mm. Figure 24 shows bigger white layer thickness and higher heat affected zone compared to the previous two samples.

The white layer thickness is attributed to the applied discharge current during the machining process, but the white layer in this case is more attributed to the pulse on time, because the large pulse on time occupied the large part of the machining cycle, which means that the pulse off time was short, resulting in more molten metals re-solidifying in the workpiece.

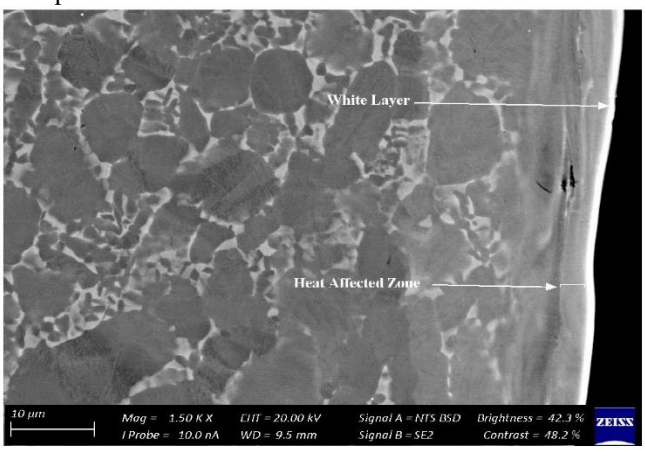

Fig. 24. SEM analysis of the heat affected zone and white layer of the machined Ti-6Al-4V with surface roughness of 3.150 µm

Again, the analysis of this preliminary sample, before the design and optimization, points out the need of optimization of machining processes and also proves that the machined samples based on the response surface methodology present better surface morphologies and micro-structure.

iii. Compositional Analysis

Figure 25, Fig. 26, and Fig. 27 show the SEM-EDS (Scan Electron Microscopy with Energy Dispersion Spectroscopy) analysis of the machined surfaces. SEM-EDS reveals the percentage range of chemical elements in Ti-6Al-4V surfaces, visualized in the adequate voltage range, counted in seconds per electron-volt (cps/eV). According to the literature Ti-6Al-4V has the following chemical composition, Ti= 89.58%, Al= 6%, V= 4%, C < 0.10%, O < 0.20%, N < 0.05%, H < 0.0125%, Fe < 0.3% [2], [13], [17], [21]. During SEM-EDS it was found that all the samples demonstrate a higher Ti content near the surface, which decreases gradually to approximately the bulk concentration. It was also observed a diffusion of chemical elements from the wire electrode to the machined samples due to the high temperatures generated during the machining process and the duration of the pulse on time [5], [22], [23], [24], [25].

Brass wire electrode is composed mainly by copper (Cu=55-90%) and zinc (Zn=10-45%), but usually it is added lead (Pb=2%), tin (Sn=1%), aluminum (Al), nickel (Ni), iron (Fe), silicon (Si) and manganese (Mn) to improve the strength, resistance to corrosion, wear and tear [23], [24], [26]. Due to the diffusion of elements during the machining process Fig. 25 reveals an addition of Cu, Si, Sn, Mn, Ca, and Zn to its original chemical composition. Figure 25 presents a sample machined at Ton=31.2 ms, I= 136 A, UHP = 217 V, with a resultant surface roughness of 0.590 μm. Due to the diffusion of elements during the machining process Fig. 25 reveals an addition of Cu, Si, Sn, Mn, Ca, and Zn to its original chemical composition. It reveals a greater number of added elements due to the discharge current and machining time for the obtained smother surface roughness, the longer machining time results in longer exposure to the high temperatures, consequently more diffusion of chemical elements to the workpiece.

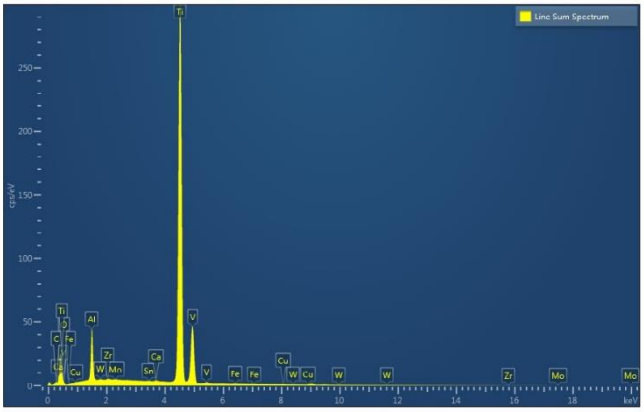

Fig. 25. SEM-EDS analysis of the machined Ti-6Al-4V with surface roughness of 0.590 μm

Figure 26 presents a sample machined at Ton=15.6 ms, I= 102 A, UHP = 326 V, with a resultant surface roughness of 1.440 μm. Due to the diffusion of elements during the machining process, Fig. 26 reveals an addition of Cu, Si, Sn, Ca, and Mn. The discharge current applied here is less than the discharge current applied in the sample of 0.590 μm, the pulse on time is shorter and the total machining time is shorter as well, this resulted in shorter exposure to the heat, thus having lower diffusion of chemical elements to the workpiece.

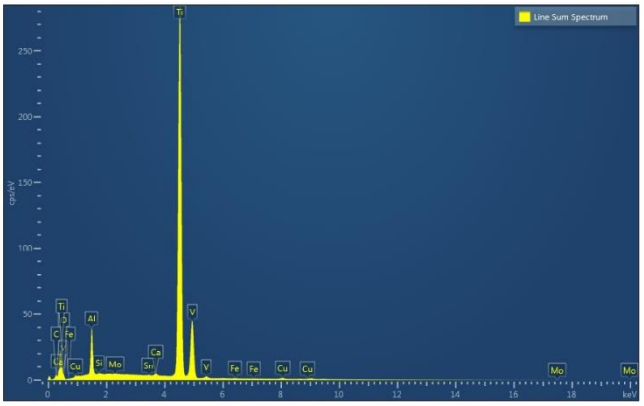

Fig. 26. SEM-EDS analysis of the machined Ti-6Al-4V with surface roughness of 1.440 µm

Figure 27 presents a sample machined at Ton=500 ms, I= 578 A, UHP = 54 V, with a resultant surface roughness of 3.150 μm. Due to the diffusion of elements during the machining process Fig. 27 reveals an addition of Cu, Si, and Ca. The added chemicals in this sample are less in number than the added chemicals in the previous two samples but just a difference of two elements with the sample in Fig. 26. This analysis highlights the aspect of machining time, although the composition is affected by the discharge current, the pulse on time during the machining, it also matters the total machining time. Considering that a rough surface like this does not need long machining time, and that wire electrical discharge machining operates at high temperatures, though the pulse on time is longer, the less the workpiece is exposed to heat, for the whole machining process, the less is the probability of diffusion of chemical elements from the workpiece to the material, which is highly influenced by the temperature.

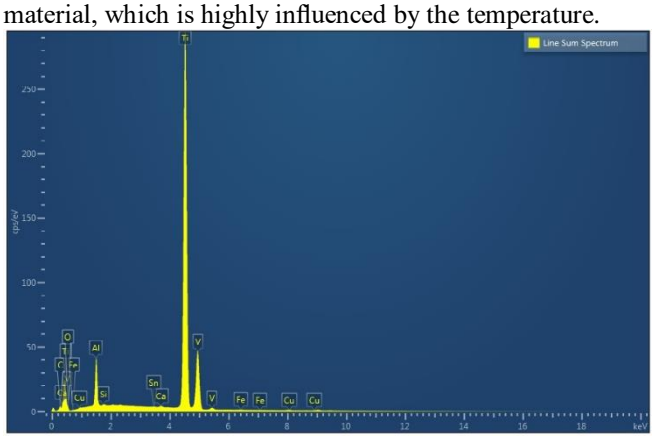

Fig. 27. SEM-EDS analysis of the machined Ti-6Al-4V with surface roughness of 3.150 µm

E. Artificial Neural Networks

A feedforward back-propagation neural network algorithm by 1-30-3 network topology was developed to predict the wire-EDM machining process parameters for surface roughness. The developed multilayer neural network has one input layer (IL), one hidden layer (HL), and one output layer (OL). Thus, corresponding to one input parameter (surface roughness), there is one neuron in the input layer, and three neurons in the output layer corresponding to the three process parameters, Ton, I, and UHP. Figure 28 presents the architecture of the developed artificial neural network model.

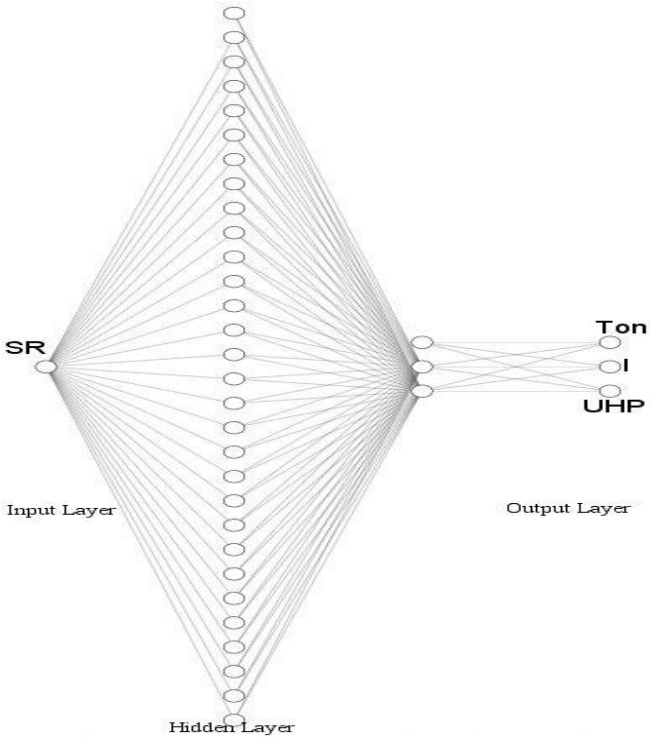

Fig.28. Architecture of the developed artificial neural networks

The model was developed and trained using built in MATLAB toolbox nntool. Figure 29 presents the MATLAB diagram of the model. Samples from the design of experiment were used to train the model. The surface roughness data was used as the input data (in the input layer) and the process parameters were used as the target data (in the output layer).

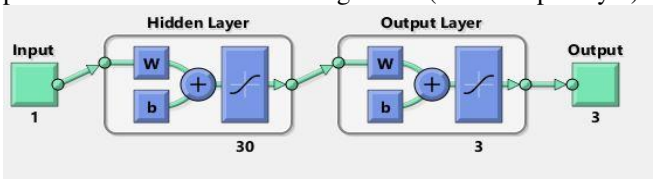

Fig. 29. MATLAB diagram of the ANN model

The model was trained using Levenberg-Marquardt training algorithm. After searching the optimal performance and a good coefficient of determination by adjusting the number of hidden layers and the number of neurons in the hidden layer, the best result attained was with one input layer, one hidden layer with 30 neurons and one output layer with 3 neurons corresponding to the three process parameters Ton, I, and UHP. The minimum gradient was reached at epoch 456 and the threshold was set at 0.000100. The analysis of the performance and reliability of the developed artificial neural network was based on the coefficient of determination or correlation coefficient (R value) of the model as presented in Fig. 30.

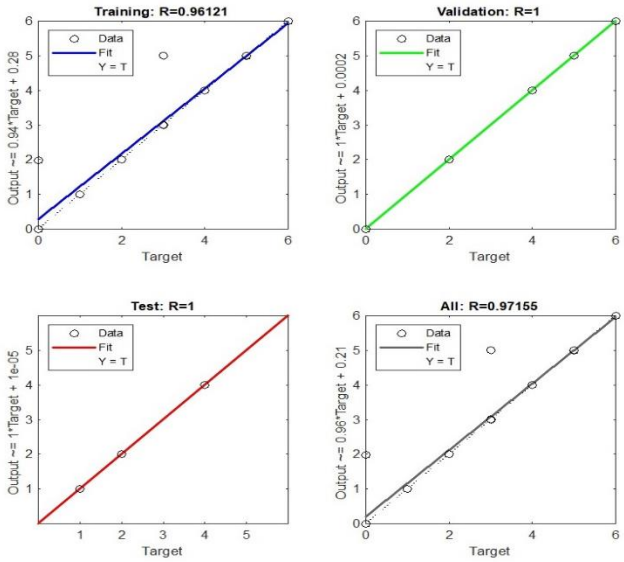

Fig. 30. Artificial Neural Network Training Regression

The correlation coefficient measures how well the model explains the change in the neural network outputs in relation to the provided target values. Its values range from 0 to 1, where 1 indicates an excellent correlation between the output and the targets [27],[28],[29]. The obtained correlation coefficient is 0.97155 which indicates a good fit of the model. This correlation coefficient confirms the significance and reliability of the developed model.

i. Confirmation Experiment

The predictive performance of the artificial neural network model was tested based on the predicted process parameters from stochastically selected experimental dataset not used in the training process and the result is given in Tab. V. The actual values were compared to the artificial neural network predicted values, and the prediction error was computed by

$$P_{error}\% = \frac{|x_a - x_p|}{x_a} * 100\%$$

where P_{error} represents the prediction error, x_a represents the actual or experimental values and x_p represents the predicted values. The minimum and maximum error recorded was 0.04% and 2.7% respectively. The maximum error in the ANN model prediction is found to be less than 10%, as per the available literature [27], [28], the model presents a satisfactory predictive capability. Table V and Fig. 31 present the data used during the confirmation experiment and the respective prediction errors.

TABLE V
Artificial neural network model confirmation experiment results

		Actual Values			Predicted Values			Error %		
Exp.	SR	Ton	I	UHP	Ton	I	UHP	Ton	I	UHP
1	0.422	31.25	102	108.57	31.46	101.3	105.63	0.68	0.683	2.705
2	0.79	15.62	136	325.71	15.21	134.52	325.16	2.61	1.085	0.168
3	0.576	15.62	102	217.14	15.35	101.43	215.33	1.75	0.55	0.833
4	0.475	15.62	136	162.85	15.86	136.23	160.9	1.55	0.172	1.196
5	0.865	15.62	102	325.71	15.65	101.95	325.01	0.17	0.046	0.215

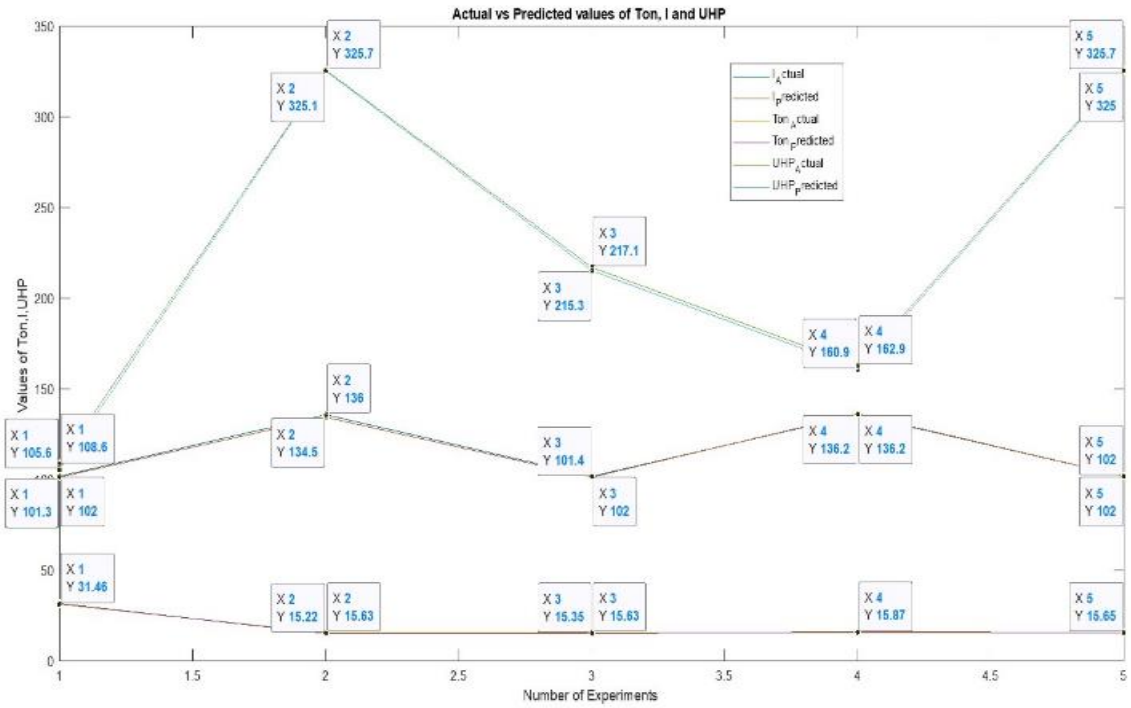

Fig. 31. Plot of the actual values vs ANN predicted values

The predictions of each process parameter were statistically analyzed using MATLAB curve fitting toolbox and values of sum of squares error (SSE), R-squared, Adjusted R-squared and root mean square error (RMSE) were obtained according to Tab. VI. As mentioned before, SSE measures how far the actual values from the predicted values. R-squared evaluates the model fit, the proportion of the data that is correctly predicted by the model, without including the degrees of freedom. The adjusted R-squared includes the degrees of freedom in its evaluation. RMSE evaluates the standard deviation of the prediction errors. The statistical analysis revealed that the error between the predicted and actual values is small and the fit of each predicted parameter is good, therefore they confirm the good prediction of the developed ANN model.

TABLE VI
Statistical analysis of the ANN predicted values

Parameters	SSE	R-squared	Adj. R-squared	RMSE
Ton	0.2579	0.9987	0.9983	0.2932
I	1.697	0.9988	0.9984	0.7521
UHP	0.1271	1	1	0.2058

V. Conlusions

This paper presents a study of the prediction of wire-EDM machining process parameters for surface roughness using Artificial Neural Network model and Response Surface Methodology, and Scan Electron Microscopy analysis of surface morphology, microstructure and composition. Based on the results, the following conclusions are drawn:

i. The two-factor interaction model developed is accurate and used successfully for the prediction of the surface roughness in relation to the investigated process parameters. The percent contributions of the input variables and interaction on the surface roughness were obtained as: Ton = 2.31%, I = 12.47%, UHP = 14.56%, TonxI = 0.76%, TonxUHP = 17.61%, IxUHP = 11.11%.

ii. The optimal parameter settings for minimum surface roughness of 0.3704 μm is pulse-on time (Ton) of 46.8 ms, discharge current (I) of 102 A, and open circuit voltage (UHP) of 108V.

iii. The analysis of variance clearly show that the open circuit voltage is the most influential parameter on the obtained surface roughness followed by discharge current. The ANOVA analysis revealed that the surface roughness of Ti-6Al-4V increases with the increase of discharge current and open circuit voltage. But the pulse on-time was found to be less effective to the obtained surface roughness.

iv. The SEM analysis confirm a change in the morphology and micro-structure of Ti-6Al-4V due to discharge current and open circuit voltage resulting in bigger crater sizes, more cracks and higher thickness of the white layer and HAZ as these parameters are increased. A higher white layer thickness result is also influenced by a longer pulse on-time.

v. Better characteristics of the morphology are obtained at lower discharge current, and open circuit voltage regarding to low surface roughness values, narrow craters, melted drops and small cracks. A white layer thickness of 0.013mm, 0.016mm, and 0.021mm and HAZ of 0.027mm, 0.043mm, and 0.081mm are observed for machined surfaces of 0,590 μm, 1.440 μm and 3.150 μm respectively.

vi. The SEM-EDS analysis confirmed the diffusion of chemical elements from the wire to the workpiece during the machining process due to the applied discharge current, longer pulse on time and total machining time.

vii. The developed artificial neural network provide prediction capability of 97.155% in the correlation coefficient and an average error of 2.845%.

viii. The confirmation experiment revealed that the predicted values are very close to the actual values, being the minimum and maximum error recorded correspondent to 0.04% and 2.7% respectively. The experiment confirmed that the developed model is accurate in predicting the process parameters for desired surface roughness and can be satisfactory used for prediction of process parameters during WEDM process.

VI. References

[1] D. Ghodsiyeh, A. Davoudinejad, M. Hashemzadeh, N. Hosseininezhad, and A. Golshan, "Optimizing finishing process in wedming of titanium alloy (Ti6Al4V) by brass wire based on response surface methodology," *Res. J. Appl. Sci. Eng. Technol.*, vol. 5, no. 4, pp. 1290–1301, 2013.

[2] A. Ram Prasad; Koona Ramji; G. Datta, "An Experimental Study of Wire EDM on Ti-6Al-4V Alloy," *Procedia Mater. Sci.*, vol. 5, pp. 2567–2576, 2014.

[3] M.M. Rahman, "Modeling of machining parameters of Ti-6Al-4V for electric discharge machining: A neural network approach," *Sci. Res. Essays*, vol. 7, no. 8, pp. 881–890, 2012.

[4] J. D. Patel and K. D. Maniya, "A Review on: Wire cut electrical discharge machining process for metal matrix composite," *Procedia Manuf.*, vol. 20, pp. 253–258, 2018.

[5] S. R. Pujari, R. Koona, and S. Beela, "Surface integrity of wire EDMed aluminum alloy: A comprehensive experimental investigation," *J. King Saud Univ. - Eng. Sci.*, vol. 30, no. 4, pp. 368–376, 2018.

[6] J. B. Saedon, N. Jaafar, R. Jaafar, N. H. Saad, and M. S. Kasim, "Modeling and Multi-Response Optimization on WEDM Ti6Al4V," *Appl. Mech. Mater.*, vol. 510, pp. 123–129, 2014.

[7] M. Altug, M. Erdem, and C. Ozay, "Experimental investigation of kerf of Ti6Al4V exposed to different heat treatment processes in WEDM and optimization of parameters using genetic algorithm," *Int. J. Adv. Manuf. Technol.*, vol. 78, no. 9–12, pp. 1573–1583, 2015.

[8] S. Shakeri, A. Ghassemi, M. Hassani, and A. Hajian, "Investigation of material removal rate and surface roughness in wire electrical discharge machining process for cementation alloy steel using artificial neural network," *Int. J. Adv. Manuf. Technol.*, vol. 82, no. 1–4, pp. 549–557, 2016.

[9] S. Ramesh, L. Karunamoorthy, and K. Palanikumar, "Measurement and analysis of surface roughness in turning of aerospace titanium alloy (gr5)," *Meas. J. Int. Meas. Confed.*, vol. 45, no. 5, pp. 1266–1276, 2012.

[10] K. Ramesh, S. Karunamoorthy, L. and Palanikumar, "Surface roughness analysis in machining of titanium alloy," *Mater. Manuf. Process.*, vol. 23, no. 2, pp. 175–182, 2008.

[11] A. Temmler, M. A. Walochnik, E. Willenborg, and K. Wissenbach, "Surface structuring by remelting of titanium alloy Ti6Al4V," *J. Laser Appl.*, vol. 27, no. S2, p. S29103, 2015.

[12] A. Gutierrez; F. Paszti; A. Climent-Font; J. Jimenez; M. Lopez, "Comparative study of the oxide scale thermally grown on titanium alloys by ion beam analysis techniques and scanning electron microscopy," *J. Mater. Res.*, vol. 23, no. 8, pp. 2245–2253, 2008.

[13] S. Ramesh, L. Karunamoorthy, and K. Palanikumar, "Fuzzy modeling and analysis of machining parameters in machining titanium alloy," *Mater. Manuf. Process.*, vol. 23, no. 4, pp. 439–447, 2008.

[14] F. Nourbakhsh, K. P. Rajurkar, A. P. Malshe, and J. Cao, "Wire electro-discharge machining of titanium alloy," *Procedia CIRP*, vol. 5, pp. 13–18, 2013.

[15] W. Ahmed and M. J. Jackson, *Titanium and Titanium Alloy Applications in Medicine*. 2016.

[16] M. P. Jahan, P. Kakavand, and F. Alavi, "A Comparative Study on Micro-electro-discharge-machined Surface Characteristics of Ni-Ti and Ti-6Al-4V with Respect to Biocompatibility," *Procedia Manuf.*, vol. 10, pp. 232–242, 2017.

[17] B. B. Pradhan and B. Bhattacharyya, "Modelling of micro-electrodischarge machining during machining of titanium alloy Ti-6Al-4V using response surface methodology and artificial neural network algorithm," *Proc. Inst. Mech. Eng. Part B J. Eng. Manuf.*, vol. 223, no. 6, pp. 683–693, 2009.

[18] M. Mäkelä, "Experimental design and response surface methodology in energy applications: A tutorial review," *Energy Convers. Manag.*, vol. 151, no. May, pp. 630–640, 2017.

[19] M. A. Bezerra, R. E. Santelli, E. P. Oliveira, L. S. Villar, and L. A. Escaleira, "Response surface methodology (RSM) as a tool for optimization in analytical chemistry.," *Talanta*, vol. 76, no. 5, pp. 965–77, 2008.

[20] D. Devarasiddappa, J. George, M. Chandrasekaran, and N. Teyi, "Application of Artificial Intelligence Approach in Modeling Surface Quality of Aerospace Alloys in WEDM Process," *Procedia Technol.*, vol. 25, no. Raerest, pp. 1199–1208, 2016.

[21] K. Maity and S. Pradhan, "Study of Chip Morphology, Flank Wear on Different Machinability Conditions of Titanium Alloy (Ti-6Al-4V) Using Response Surface Methodology Approach," *Int. J. Mater. Form. Mach. Process.*, vol. 4, no. 1, pp. 19–37, 2017.

[22] K. . Maity and M. . Mohanta, "Modeling of micro wire electro discharge machining in aerospace material," *Proc. 7th AWMFT*, vol. 008, p. CD-ROM, 2014.

[23] A. Pramanik, A. K. Basak, and C. Prakash, "Understanding the wire electrical discharge machining of Ti6Al4V alloy," *Heliyon*, vol. 5, no. 4, p. e01473, 2019.

[24] G. Cao, G. Chi, B. Jin, Z. Wang, and W. Zhao, "Micro EDM deposition by using brass wire electrode in air," *Am. Soc. Mech. Eng. Manuf. Eng. Div. MED*, vol. 16–2, pp. 953–956, 2005.

[25] G. Zhang, Z. Chen, Z. Zhang, Y. Huang, W. Ming, and H. Li, "A macroscopic mechanical model of wire electrode deflection considering temperature increment in MS-WEDM process," *Int. J. Mach. Tools Manuf.*, vol. 78, pp. 41–53, 2014.

[26] J. Kapoor, J. S. Khamba, and S. Singh, "Effect of different wire electrodes on the performance of WEDM," *Mater. Sci. Forum*, vol. 751, pp. 27–34, 2013.

[27] G. Kant and K. S. Sangwan, "Predictive modelling and optimization of machining parameters to minimize surface roughness using artificial neural network coupled with genetic algorithm," *Procedia CIRP*, vol. 31, pp. 453–458, 2015.

[28] G. Ugrasen, H. V. Ravindra, G. V. N. Prakash, and R. Keshavamurthy, "Process Optimization and Estimation of Machining Performances Using Artificial Neural Network in Wire EDM," *Procedia Mater. Sci.*, vol. 6, no. Icmpc, pp. 1752–1760, 2014.

[29] A. M. Khorasani and M. R. S. Yazdi, "Development of a dynamic surface roughness monitoring system based on artificial neural networks (ANN) in milling operation," *Int. J. Adv. Manuf. Technol.*, vol. 93, no. 1–4, pp. 141–151, 2017.